Industrial Crops & Products 236 (2025) 122031

Contents lists available at ScienceDirect

Industrial Crops & Products

journal homepage: www.elsevier.com/locate/indcrop

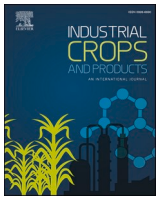

Cascade biorefinery approach to obtain hemicelluloses, lignin, cellulose and nanocelluloses from high-yield forest crops (*Ulmus minor*) for different industrial applications

J.M. Loaiza [a,*], E.A. Gutiérrez [b,c], J.C. García [a], F. López [a]

[a] *Department of Chemical Engineering, University of Huelva, Research Centre for Technology of Products and Chemical Processes (PRO²TECS), Av. 3 de marzo s/n, Huelva 21071, Spain*

[b] *Agri-Food Research and Development Laboratory – LIDA, School of Basic Sciences, Technology and Engineering, National University Open and Distance (UNAD), Bogotá D.C, Colombia*

[c] *Escuela de Ciencias Básicas, Tecnología e Ingeniería (ECBTI), Universidad Nacional Abierta y a Distancia (UNAD), 680001, Bucaramanga, Santander 680002, Colombia*

ARTICLE INFO

Keywords:
Biorefinery
Cellulose
Cold alkaline extraction
Elm
Nanocelluloses

ABSTRACT

An Elm clone (*Ulmus minor)* is evaluated as a renewable lignocellulosic feedstock for a cascade biorefinery. Hemicelluloses are selectively extracted by Cold Alkaline Extraction (CAE), and the cellulose-rich residue is subsequently delignified and converted into cellulose nanofibers (CNFs). Two post-CAE treatments—alkaline hydrogen peroxide (AHP) delignification and TEMPO-mediated oxidation—are employed, and their effects on CNF physicochemical properties are assessed using FTIR, SEM, ζ-potential, conductometric titration, and thermogravimetric analysis. The combination of CAE and AHP effectively removes lignin and hemicellulose, paving the way for subsequent TEMPO oxidation to modify the fiber surface. FTIR analysis confirms the successful removal of these components, while SEM imaging reveals the structural transformations in the fibers after treatment. Techniques such as ζ-potential measurement and conductometric titration, used in conjunction, provide insight into the surface charge and degree of carboxylation, respectively. These measurements indicate enhanced dispersion stability and the effectiveness of surface modification. TGA highlights the influence of chemical pretreatment on thermal stability, with nanofibers of cellulose exhibiting distinct degradation profiles compared to untreated fibers. Collectively, these findings underscore the importance of a multi-faceted approach for optimizing the properties of cellulose nanofibers. By tailoring the pretreatment process, researchers can achieve desired characteristics for diverse applications.

1. Introduction

International agreements on climate change, signed by Spain and the European Union, have promoted the adoption of renewable, sustainable sources of energy, including biomass, to mitigate greenhouse gas emissions and better protect the global environment (Council of the European Union. 2023). Biomass has been recognized as a flexible energy source for this purpose due to its ability to produce high-value products, such as pellets, biogas, and syngas, as well as useful chemicals, through biorefining (Council of the European Union., 2023; International Energy Agency (IEA), 2017). However, many agroforestry systems by themselves cannot meet the increasing demand for biomass from agricultural and forestry residues. Planting fast growing plant species may help meet the requirements for additional ligneous biomass and expand the biomass market by facilitating the alternative use of waste land, thereby improving social and economic development in rural areas while reducing production of atmospheric CO_2 (Alaejos et al., 2023; Alesso et al., 2021; Fernández et al., 2018; Fernández et al., 2020; International Energy Agency (IEA), 2017).

A recent study conducted by the Committee on Agriculture and Rural Development (AGRI, European Parliament, 2020) found that roughly 30 % of all useful agricultural land in the EU-27 (i.e., 56 million hectares) is at a moderate to high risk of being abandoned. About 5 million hectares are expected to become unused by 2030 (EP AGRI, 2020). In Spain, with a dryland area of around 13 million hectares (MTERD Ministerio para la Transición Ecológica y el Reto Demográfico, 2022),

* Corresponding author.
E-mail address: javiermauricio.loiza@diq.uhu.es (J.M. Loaiza).

https://doi.org/10.1016/j.indcrop.2025.122031
Received 25 March 2025; Received in revised form 27 September 2025; Accepted 29 September 2025
Available online 6 October 2025

more than 0.4 million are expected to be at risk of abandonment by 2030, and over 4 million in the longer term.

Deleterious effects such as reduced soil fertility from the removal of nutrients and habitat and biodiversity changes in sensitive areas may be mitigated by using short-rotation scrubland plantations of fast-growing woody species to sustainably produce biomass in a short period (Bessaad et al., 2021; Srirangan et al., 2012).

Several short-rotation scrubland taxa are currently used worldwide for energy production from woody biomass, known as "energy crops." These include the genera *Populus, Salix, Eucalyptus, Paulownia, Gmelina, Casuarina,* and *Leucaena*, as well as species such as *Ulmus pumila L. (Siberian elm), Robinia pseudoacacia L. (black locust), Platanus hispanica -Mill. ex Münchh*, and *Ailanthus altissima -Mill Swingle*. Most of these are multipurpose species that yield between 15 and 40 tons of dry matter annually under optimal conditions in commercial plantations (Feria et al., 2012; Sixto et al., 2015; Oliveira et al., 2018; Fernández et al., 2018, 2020, 2023; Loaiza et al., 2019, 2020; Nicolescu et al., 2020; Amorós et al., 2021; Alesso et al., 2021; Alaejos et al., 2023).

Recent studies have shown *Robinia pseudoacacia, Ulmus pumila, and Populus sp.* to be especially useful in Mediterranean continental climates with cold winters in Central Europe and North America, where they tolerate temperatures below −20 °C (Pérez et al., 2014; Oliveira et al., 2018; Vanbeveren et al., 2015; Alesso et al., 2021). The genus Populus can easily grow in a variety of environmental conditions and has high hydration capacity and plant propagation ability. However, it requires wet soil to grow. Conversely, Robinia pseudoacacia and Ulmus pumila are especially tolerant to drought (Sixto et al., 2015; García, 2016; Oliveira et al., 2018).

Biorefinery schemes enable renewable and sustainable lignocellulosic resources to be processed industrially to obtain fractions with new, innovative uses. Of particular interest are two-step fractionation schemes (Ferreira et al., 2018), which allow the extraction of minority fractions (e.g., hemicelluloses) through cold alkaline extraction (CAE) under relatively mild conditions to reduce degradation of cellulose fibers, and alkaline hydrogen peroxide delignification of the residual solid. Several methods have been reported to utilize the two fractions (solid cellulosic fraction and the rich hemicellulose and lignin liquid fraction) for producing valuable chemicals (Yetiş et al. 2020; Sánchez et al., 2011). A viable method for valuing the solid cellulosic fraction from rapidly expanding plantation biomass within a biorefinery framework is to combine CAE fractioning with TMO-based preparation. A solid post-CAE fraction of high-quality cellulose pulp is produced by the selective extraction of hemicelluloses made possible by CAE. For the TMO-based synthesis of nanocellulose, this cellulose pulp is essential. Cellulose nanofibrils (CNFs), which have superior physicochemical properties like high crystallinity and thermal stability and are suitable for a range of industrial and medicinal applications, are created by oxidizing the C6 hydroxyl groups in cellulose through the TMO process. This sequential approach not only maximizes the utilization of fast-growing plantations biomass but also aligns with the ideas of green chemistry and the circular economy, providing a productive and sustainable way to make valuable materials. (Velvizhi et al., 2022; Domínguez et al., 2020; Li et al., 2017; Reiner and Rudie, 2017).

Nanocellulose, characterized by cellulose molecules with dimensions ranging from 1 to 100 nanometers, has become a focal point in nanotechnology. Its appeal lies in the ability to create a uniform material with enhanced physicochemical and mechanical properties simply by reducing the size of cellulose fibers (Faradilla et al., 2020; Salas et al., 2014). Although cellulose units are naturally strong, defects are introduced during the assembly process, producing weaker fibers with reduced theoretical strength. But compared to their parent fibers, extracted nanocellulose offers superior mechanical strength, barrier properties, and biodegradability compared to other materials (Reshmy et al., 2021).

Mostly derived from lignocellulosic biomass, nanocellulose also comes from many agricultural and food-based waste sources. It provides outstanding qualities including biodegradability, biocompatibility, increased firmness, strength, and reduced density. Particle size is the main difference between cellulose and nanocellulose; the latter shows lower density and more crystallinity. Nanocellulose can be categorized into three main types: nanocellulose crystals (NCC) (Lokanathan et al., 2014), cellulose nanofibers (CNF) (Nechyporchuk, 2015), and bacterial nanocellulose (BNC) (Torres et al., 2019). From food-related uses to packaging materials, biosensors, 3-D printing hydrogels, and emulsion stabilizers, nanocellulose's many possible uses reflect its adaptability. Despite its advantages, nanocellulose is not yet extensively commercially available. Its more general acceptance is hampered by issues including high production costs, increased energy consumption, environmental and human health safety issues.

The most researched technique for producing nanocellulose is TMO, which uses sodium hypochlorite (NaClO) as an oxidant, sodium bromide (NaBr) as a co-catalyst, and 2,2,6,6-tetramethyl-1-piperidinyloxy (TEMPO) as a catalyst. (Mishra et al., 2011; Li et al., 2017). Cellulose nanofibrils (CNFs) can be produced by this process from a range of materials including husks, coconut shells, and reed stalks. The CNFs produced have improved physicochemical properties such as surface functionalities, thermal properties, and crystallinity. The TMO process has also been optimized to increase CNF production efficiency while reducing the consumption of TEMPO and NaBr, making it a versatile and sustainable green platform for the production of nanocellulose. The mechanism of TMO consists of oxidizing the C6 hydroxyl groups of cellulose to aldehyde groups and subsequently to carboxyl groups at a specific pH and ambient temperature. Introducing carboxylic groups through TMO promotes electrostatic repulsion at the surface of the fibrils, making subsequent mechanical processes more efficient. This has led to substantial savings in TEMPO and NaBr compared to conventional process conditions, as well as a reduction in oxidation time and effluent volume. In this work, an Elm clone (viz., *Ulmus minor*) was assessed to obtain hemicelluloses by CAE and to produce nanocellulose.

2. Materials and methods

2.1. Raw materials, characterization and storage

The raw material used was wood of clone Elm (viz., *ulmus minor*). The wood was obtained from plants harvested at 3-yr intervals from a crop grown over 9 years under favourable pedoclimatic, irrigation and fertilization conditions in the province of Huelva, (SW Spain). The material was sieved to obtain chips 1–3 cm long and 0.5 cm wide that were allowed to adjust to humidity and ambient temperature prior to storage in tightly-closed containers until the wood chips will been used in the CAE process. Chips were further ground to a size less than 0.5 mm, before characterization using an IKA MF 10 Basic mill (IKA®-Werke GmbH & Co. KG, Staufen, Germany). Tests were conducted in accordance with international standards including TAPPI, T264 cm-07 (2007) for moisture, TAPPI 211 om-02 (2002) for ash, and TAPPIT204-om-07 in combination with Soxhlet extraction (95 % ethanol, 5 h) for extractives.

Following gravimetric testing, the material was subjected to quantitative acid hydrolysis with 72 % H_2SO_4 and the hydrolysate analysed for glucose, xylose and arabinose (monomeric sugars) according to TAPPI T249-cm-09, using high performance liquid chromatography HPLC (Bio-Rad Laboratories, USA) with an Aminex HPX-87H ion--exchange column at 30 °C as stationary phase and 0.005 M H_2SO_4 at a flow-rate of 0.6 mL min^{-1} as mobile phase. Klason lignin was determined according to TAPPI, T222 om-11 (2011).

2.2. Cold alkaline extraction (CAE)

Raw material was subjected to CAE in a 10 L stainless steel reactor from M/K Systems, Inc. (Danvers, MA) equipped with a recirculation pump. A liquid/solid ratio of 15 Kg water per kg raw material on a dry basis (odb) was used. Temperature (20, 30 or 40 °C), time (30, 60 or

90 min) and sodium hydroxide concentration (80, 100 or 120 g/L) were the independent variables of the process. The ensuing CAE liquor was filtered and the solid residue containing the cellulosic fraction washed with water. The solid was weighed to calculate the yield of the process (after being air-dried and moisture determination). The solid fraction was characterized in chemical terms by using the same tests as with the raw material.

2.3. Experimental design, modelling and optimization by multiple regression

The CAE process was modelled by multiple regression of independent variables (with linear, quadratic and interaction terms):

$$Y = a_0 + \sum_{i=1}^{n} b_i X_{ni} + \sum_{i=1}^{n} C_i X_{ni}^2 + \sum_{i=1}^{n}\sum_{i=1}^{n} d_{ij} X_{nj} X_{nj} \; (i < j)$$

The required number of tests needed was reduced and covariance between variables decreased by using a central composition design with N tests, defined as $N = 2^{n} + 2{\cdot}n + n_c$, where 2^{n} represents he number of points constituting the design, $2{\cdot}n$ corresponds to the axial points, and n_c to the central points. Additionally, to eliminate the effect of the different ranges spanned by the variables, their values were normalizing to 0, 1 and –1 using the following equation:

$$X_n = \frac{X - \overline{X}}{(X_{max} - X_{min})/2}$$

Where X, $\overline{X}$, X_{max} and X_{min} are the value of the particular independent variable, and its mean, maximum and minimum value, respectively. The dependent variables examined were yield, glucan, xylan, Klason lignin. Only those terms with $p < 0.05$ in Student's t-test or spanning a confidence interval less than 90 % were assumed to be statistically significant and included in the equations for Y. Also, all modelling was done with the software Statistica v. 10.0 (StatSoft, Inc., Tulsa, OK, USA).

2.4. Pulping process and isolation of cellulose nanofibrils (CNFs)

After the CAE process, an alkali delignification was completed using the following conditions: alkali concentration, 21 % (on dry wood weight); temperature, 175 °C; and operating time of 60 min. However, the amount of water needed to impregnate the material was much smaller than that used for CAE, and the liquid/solid mass ratio of 8:1 was used. As in the CAE tests, recycling the liquor ensured efficient mixing and uniform delignification of the previously hydrolysed wood chips. Cellulose pulps, obtained from the solid phase after CAE, were collected in the same reactor used for the CAE pretreatment. Additionally, a pulp without CAE was processed under the same operating conditions as a reference experiment.

2.5. Isolation of cellulose nanofibrils (CNFs)

2.5.1. Alkaline hydrogen peroxide (AHP) treatment

To effectively remove residual non-cellulosic components such as hemicellulose and lignin following the CAE process, 8 g of purified and size-reduced solid phase after CAE in a Retsch mill. The material was sieved to 1–2 mm were suspended in 100 mL of a 10 % (w/w) H_2O_2 solution. The solution's pH was then adjusted to 11.5 by the dropwise addition of a 2 M NaOH solution under continuous manual stirring for 2 h at 25 °C. This treatment is referred to as Alkaline Hydrogen Peroxide (AHP) treatment. The resulting material was thoroughly washed with distilled water and oven-dried at 60 °C until constant weight was achieved.

2.5.1.1. TEMPO-mediated oxidation. A slightly modified procedure reported by Ovalle et al. (2018) was employed for the subsequent TEMPO-mediated oxidation. 1 g of the AHP-treated material, estimated to contain over 80 % cellulose, was hydrated in 100 mL of water. In a separate container, 16 mg of TEMPO radical and 100 mg of NaBr were dissolved in 50 mL of distilled water. This solution was then slowly added to the pre-hydrated material under continuous stirring at 500 rpm and maintained at 25 °C throughout the reaction. After achieving a homogeneous mixture, 0.037 mol of NaClO was added dropwise to initiate the oxidation reaction. The solution's pH was maintained between 11 and 10.5 during the process by controlled addition of either 0.5 N NaOH or 0.5 N HCl. The reaction was considered complete after approximately 2 h, indicated by a stable pH. The oxidation was then quenched with the addition of ethanol, roughly half the volume used for NaClO.

2.5.1.2. Isolation and purification of CNFs. The oxidized suspension was centrifuged at 5000 rpm for 15 min. The initial supernatant was decanted and discarded, and the pellet was resuspended in deionized water and centrifuged twice more under the same conditions. The supernatants (translucent suspensions of CNFs) from the second and third cycles were combined, while the final pellet (containing coarse, unfibrillated fibers) was discarded. The combined supernatants were probe-sonicated (20 kHz, 750 watts, and 40 % amplitude) for 10 min to complete nanofibrillation, then centrifuged once more (5000 rpm, 15 min) to remove residual aggregates. The resulting translucent dispersion was stored at 4 °C for subsequent FTIR, SEM, ζ-potential, conductometric titration, and TGA analyses.

2.5.1.3. Characterization of CNFs. The chemical composition of the CNFs was confirmed from Attenuated-Total-Reflectance Fourier-Transform Infrared (ATR-FTIR) spectra collected on a Bruker Invenio-X equipped with a diamond ATR crystal and a DTGS detector. Spectra were recorded from 4000 to 400 cm^{-1} at 4 cm^{-1} resolution, averaging 32 scans per sample. FTIR spectra were processed in OPUS software to convert the raw transmittance data to absorbance, and second-derivative peak heights were then measured (without further normalization) to calculate the total crystallinity index TCI $= A_{1373}/A_{2900}$, hydrogen-bonding index HBI $= A_{3350}/A_{1337}$, and lateral order index LOI $= A_{1427}/A_{895}$ (Kruer-Zerhusen et al., 2018). Scanning Electron Microscopy (SEM) images were obtained using a JSM-IT800HL from JEOL (Tokyo, Japan), operating in high-vacuum mode at an accelerating voltage of 1–3 kV and a working distance of approximately 5–6 mm. Freeze-dried fibers/nanofibers were mounted on aluminum stubs with double-sided carbon tape; no conductive Au/Pd sputter coating was applied to prevent artificial thickening of the nanofibrils. Before imaging, the chamber pressure was stabilized below 5×10^{-4} Pa to reduce beam-induced charging. Representative micrographs were captured with a secondary-electron detector at magnifications ranging from 10,000 × to 50,000 × and processed with ImageJ for diameter distribution analysis. Colloidal stability of nanofiber suspensions was quantified through zeta-potential analysis of 0.025 % (w/v) suspensions prepared in deionized water. The carboxyl content (surface charge) of CNFs was determined by conductimetric titration. 50 mg of nanofibres were protonated in 0.01 M HCl (pH 2) and titrated with 0.01 M NaOH. The conductivity curve shows three regions: (i) a sharp drop as NaOH neutralises free HCl, (ii) a slower decline while carboxyl groups react, and (iii) a rise once all acids are neutralised and excess NaOH accumulates. The NaOH volume consumed in region (ii) is used to calculate the degree of oxidation (DO) and carboxyl content following the equations reported by Plengnok, Jarukumjorn, (2020); Gupta et al., (2019). Finally, the thermal stability of CNFs was also evaluated through thermogravimetric analysis (TGA) under nitrogen atmosphere, ranging from room temperature to 500 °C at a heating rate of 10 °C/min.

3. Results and discussion

The starting hypothesis for this work was that cold alkaline

extraction (CAE) of elm wood would allow more efficient and selective extraction of hemicelluloses into the liquor than other pretreatments such as autohydrolysis or acid hydrolysis. The CAE treatment was examined with a view to maximizing hemicellulose extraction, and optimizing subsequent delignification and obtainment of high-purity cellulose.

3.1. Raw material characterization

Elm is a tree species spanning a wide variety of clones (EUFORGEN.. 2025). In this work, we studied a fast-growing, easily adapted clone that provides more than when harvested each 3 years 25 ton dry biomass ha^{-1} $year^{-1}$. The biomass used here consisted largely (67.4 %) of trunks and branches 2.5 −10.0 cm thick. The bark content of the biomass, which was as low as possible in order not to detract from quality, ranged from 20 −25 % in the thickest trunks to 12 % in those 5.0 −10.0 cm thick. The main reason for choosing this specific elm clone was the high sustainability of its crops. In fact, after 9 years the target plantation has substantially improved the quality of the soil by increasing its content in organic matter by 0.23 % percentage points (from the typical 0.80 % in porous soils to 1.03 %), and that in nitrogen by 0.03 % percentage points (from 0.12 % to 0.15 %).

Table 1 shows the chemical and energy-related properties of elm chips and compares them with those for other, previously studied lignocellulosic materials. The main fraction consisted of cellulose, measured as glucan; followed in content by Klason lignin (25.52 % after quantitative acid hydrolysis); and hemicellulose, measured as xylan, arabinan, acetyl groups and other, undefined compounds, which accounted for 18 % of the material.

Comparing the values for elm with those for other raw materials (Table 1) reveals that the former was very similar in glucan content to the other raw materials; also, it had one of the highest lignin Klason contents and the lowest proportion of hemicellulose —which in no way detracts from its potential as it can facilitate CAE and increase the nanocellulose yield as a result. In addition, the elm clone had a high calorific power relative to the other materials and eucalyptus, which is one of the most widely used species for energy production by boiler combustion on the grounds of its reduced hemicellulose content.

3.2. Cold alkaline extraction of hemicelluloses

Table 2 shows the extraction yield, and the amounts of glucan, xylan, lignin and hemicellulose obtained at each point of the experimental design for the CAE process. The results were modelled by using equations 1 −5 in Table 3 as described in the Methods section. Based on the differences between the experimental (observed) values and those predicted by the polynomial equations, the prediction errors were all less than 15 % —or even less than 10 % in some cases. Also, the quadratic regression coefficients, R^2, were all higher than 90 % and deemed acceptable because they were calculated simultaneously for several independent variables. Snedecor's *F*-values were all greater than 5, which is the minimum value for a fitting to be deemed accurate. All independent variables present in the models had individual Student's *t*-values above 2 or *p*-values below 0.05; therefore, the differences were all statistically significant at the 95 % level. For easier interpretation, the polynomial equations were used to generate the response surfaces shown in Fig. 1.

From the data of Tables 2 and 3 it follows that the process used to isolate the lignocellulosic fractions was efficient and also that elm is a suitable raw material for obtaining valorizable fractions.

As can be seen, the temperature was the individual CAE variable most strongly influencing the solid yield (eq. 1), glucan content (eq. 2), xylan content (eq. 3) and hemicellulose removal efficiency (eq. 5). On the other hand, the alkali concentration was the most influential variable on Klason lignin (eq. 4). By contrast, the treatment time was the least influential variable under all CAE operating conditions.

Fig. 1 shows the response surfaces constructed from the previous equations to identify the operating conditions maximizing extraction of hemicelluloses. The graphs show two surfaces each corresponding to the extreme values of the most influential independent variable and those in the studied range for the other two variables.

As can be seen from Table 2, the CAE yield was considerably higher than the values previously reported by other authors (Fernandez et al., 2020; Carvalho et al., 2016) for eucalyptus (3.2 −5.0 %) but lower than those for a grass crop such as wheat (25.5–38.8 %; (García et al., 2013). A decreased yield suggests increased extraction into the liquor. These results are consistent with the comment in the Introduction that CAE efficiency depends on the particular raw material. Thus, eucalyptus wood, which is difficult to fractionate by CAE (Carvalho et al., 2016), can be efficiently extracted at high enough temperatures such as those previously used by Loaiza et al. (2016) or Carvalho et al. (2016) —up to 180 °C, which provided yields of 10 −35 %. The differences in the polymers extracted by CAE further confirm the hypothesis.

Based on eqs 1 and 5 in Table 3, the temperature was the operational variable most markedly influencing the extraction yield. Let us first examine the yield, expressed as a proportion of solid in the starting raw material, and the proportions of Klason lignin, hemicelluloses and glucan relative to it.

The CAE solid yield was 75.2 −78.9 % on a dry matter basis of the content in the original raw material. The proportion of Klason lignin after CAE ranged from 87.8 % to 99.9 %. Therefore, most of this component remained in the solid fraction and only 0.1 −12.% was extracted. These results are quite good since the aim was to efficiently separate the lignin-containing solid fraction from the hemicellulose-

Table 1
Higher calorific value (HCV) and chemical composition of *Elm (Ulmus minor)* and other materials.

Composition	(1)	(2)	(3)	(4)	(5)	(6)	(7)	(8)
α Cellulose (glucan) (%)	39.1 ± 1.63	40.3 ± 0.85	38.9 ± 3.4	38.0 ± 2.4	44.0 ± 3.3	42.8 ± 2.0	33.8 ± 1.6	55.4 ± 2.6
Klason Lignin (%)	25.5 ± 0.12	25.1 ± 0.16	19.8 ± 1.9	19.0 ± 2.5	27.8 ± 1.1	21.2 ± 0.9	19.9 ± 0.5	16 ± 0.3
Xylan (%)	13.35 ± 0.31	19.3 ± 0.09	19.9 ± 1.3	15.7 ± 0.1	15.7 ± 0.2	17.1 ± 0.3	23.9 ± 0.1	34.6 ± 0.4
Arabinan (%)	2.62 ± 0.08	———	0.6 ± 0.3	1.5 ± 0.3	1.1 ± 0.1	0.7 ± 0.1	0.37 ± 0.2	5.6 ± 0.3
Acetyl groups (%)	1.86 ± 0.04	0.7 ± 0.02	4.4 ± 0.6	3.3 ± 0.5	4.4 ± 0.2	3.5 ± 0.1	4.32 ± 0.1	———
LHV, KJ/kg odb, over dry basis.	20760 ± 35	19982 ± 30	19592 ± 28	18981 ± 95	20300 ± 53	19326 ± 84	17259 ± 25	———

Raw material percentages (100 kg dry matter)
1-Elm *(ulmus minor)*. Present study (1)
2- Genus *Populus*. Lozano-Calvo et al., (2024) (2)
3- Tagasaste (*Chamaecytisus proliferus*). Alfaro et al., (2010)) (3)
4- Leucaena (*Leucaena diversifolia)*. Feria et al., (2012) (4)
5- *Paulownia trihybrid*. López et al., (2012) (5)
6- *Eucalyptus globulus*. Loaiza et al., (2016) (6)
7- Sunflower stalks. Caparrós et al., (2008) (7)
8- Wheat straw. Pan, Sano (2005) (8)

Table 2
Normalized values of the independent variables (alkali concentration, XA; treatment time, Xt; and temperature, XT) and composition of the solid fractions obtained in the cold alkaline extraction (CAE) of the *Elm (Ulmus minor)*. The glucan, xylan and lignin contents are percentages relative to the raw material. * Total hemicellulose extraction (xylan, arabinan, and acetyl groups) in the liquid phase, expressed as a percentage of their initial content in the raw material.

Variables							
X_A	X_t	X_T	Yield (%)	Glucan (%)	Xylan (%)	Klason Lignin (%)	*Total Hemicelluloses Extracted (%)
0	0	0	75.2	82.4	53.2	93.9	51.3
0	0	0	75.3	81.6	54.8	92.0	49.7
1	1	1	76.5	91.5	57.7	97.6	46.8
1	1	−1	78.9	90.0	63.1	99.9	41.4
1	−1	1	76.3	93.5	58.0	95.2	46.5
1	−1	−1	78.6	83.8	60.3	91.3	44.2
−1	1	1	75.4	93.7	54.0	87.8	50.5
−1	1	−1	77.8	89.3	57.4	88.3	47.0
−1	−1	1	76.6	90.1	52.6	91.9	51.8
−1	−1	−1	78.4	87.2	58.2	91.1	46.3
1	0	0	77.1	83.8	59.6	95.2	44.9
−1	0	0	76.8	84.9	56.9	89.3	47.6
0	1	0	76.3	90.1	52.1	93.6	52.4
0	−1	0	76.6	83.2	50.5	91.5	54.0
0	0	1	76.5	82.0	41.8	89.1	64.3
0	0	−1	78.2	78.4	48.3	90.5	56.2

Table 3
Equations of the polynomial models for the dependent variables of the cold alkaline extraction (CAE).

	Eq. N°.	Equation	Adjusted R^2	Snedecor's F
Cold Alkaline Extraction	1	$YI = 75.51 + 0.24X_A - 1.05X_T + 1.16\ X_AX_A - 1.14X_tX_t + 1.83X_T\ X_T + 0.29X_A\ X_t$	0.92	31.2
	2	$GL = 81.09 + 2.20X_T + 1.46X_t + 3.27\ X_AX_A + 5.53X_t\ X_t - 1.06X_t\ X_T$	0.90	29.3
	3	$X = 53.33 + 1.94X_A - 2.48X_T - 5.53X_AX_A + 7.71X_tX_t - 9.09X_TX_T$	0.94	49.3
	4	$KL = 92.62 + 3.07X_A + 3.01X_tX_t - 2.82X_TX_T + 2.23X_AX_t - 0.95\ X_TX_t$	0.94	34.4
	5	$THE = 51.14 - 1.94X_A + 2.48X_T - 5.53X_AX_A - 7.71X_tX_t + 9.09X_TX_T$	0.94	49.3

Dependent variables: YI yield (%), GL glucan (%), X xylan (%), KL Klason lignin (%), THE total hemicellulose extracted (%). Independent variables: X_t (time), X_T (temperature), X_C (alkali concentration). All expressed in coded units.
Variation coefficient between experimental and calculated values are < 10 %.

containing liquor.

The glucan content of the post-CAE solid residue was also relatively high (78.4 −93.7 %). Therefore, only 6.3 −21.6 % of the amount present in the starting raw material was present in the liquor.

The xylan content in the post-CAE solid residue was 41.8 −63.1 % and the remainder (39.7 −58.2 %) was present in the liquor.

The other two hemicellulosic components (viz., araban and acetyl groups) were quantitatively extracted into the liquor since neither was present in the post-CAE solid.

As can be seen from Figs. 1a and 1b, values in the upper range of the most influential variable (temperature) led to the highest glucan contents and lowest xylan contents in the post-CAE solid. This result suggests especially selective extraction of the polyphenol and hemicellulose fractions into the liquor. The glucan content in the post-CAE solid peaked at the ends of the operational values for the other two independent variables, and so did the glucan content at the central values of the treatment time.

The differences in xylan content at the 0 0 0 point of the experimental design for the whole sampling space were relatively small, which suggests that a low degree of polymerization and crystallinity facilitated decomposition into monosaccharides and their extraction into the liquor. In fact, a comparison of the experimental ranges for the extraction of hemicelluloses, as xylan (44.3–60.8 %), and the predictions of eqs 3 (59.8 %) and 5 (54.8 %), reveals that CAE was much more selective for the hemicellulose fraction (xylan) than it was for the glucose fraction (glucan). Interestingly, these results suggest that CAE is highly selective towards hemicelluloses but preserves glucan integrity. Alkaline treatments usually alter the lignocellulosic material by reducing the degree of polymerization and crystallinity of cellulose, thereby decreasing its inner area and facilitating its release in the extraction medium (Haldar and Purkait, 2020; Schild et al., 2010).

Based on the previous results, maximizing hemicellulose extraction into the liquor while preserving glucan integrity requires using a long treatment time in combination with a medium temperature and alkali concentration.

As shown in Fig. 1c, the proportion of lignin in the post-CAE solid residue increased at high alkali concentrations, medium to high temperatures, and long treatment times. However, CAE is known to have a slight delignification effect, and differences in contents may arise from extractability differences in other fractions. In fact, the extent of delignification at the 0 0 0 point of the experimental design was estimated to be 7.4 % (Table 3), and the total proportion ranged from 1.0 % to 11.7 % (Table 2). In any case, lignin was invariably extracted to a lesser extent than were hemicelluloses, which suggests that CAE was less selective towards the lignin fraction. Overall, prolonged times in combination with medium alkali concentrations and moderate temperatures resulted in post-CAE solid residues with the highest glucan and lignin contents. As shown in Fig. 1d, the proportion of hemicelluloses extracted into the liquor increased with high temperatures and moderately long treatment times. This result suggests that the CAE efficiency not only depends linearly on the operational variables, but also on a combination that maximizes hemicellulose extraction into the liquor.

3.3. Pulping process and isolation of cellulose nanofibrils (CNFs)

The delignification processes and subsequent isolation of cellulose nanofibers have been carried out on the post-CAE solid fraction obtained under the conditions indicated as "optimal" in the previous section.

Following CAE of Elm samples, an additional pretreatment with alkaline hydrogen peroxide (AHP) was employed further to solubilize residual lignins and hemicelluloses within the lignocellulosic material. This process aimed to isolate a purer cellulose fraction as a solid residue. According to the "Alkaline Hydrogen Peroxide (AHP) Treatment" section, the conditioned Elm-CAE samples were contacted with a 10 % (v/v) H_2O_2 solution at pH 11.5 in a 1:2 (w/v) biomass-to-solution ratio

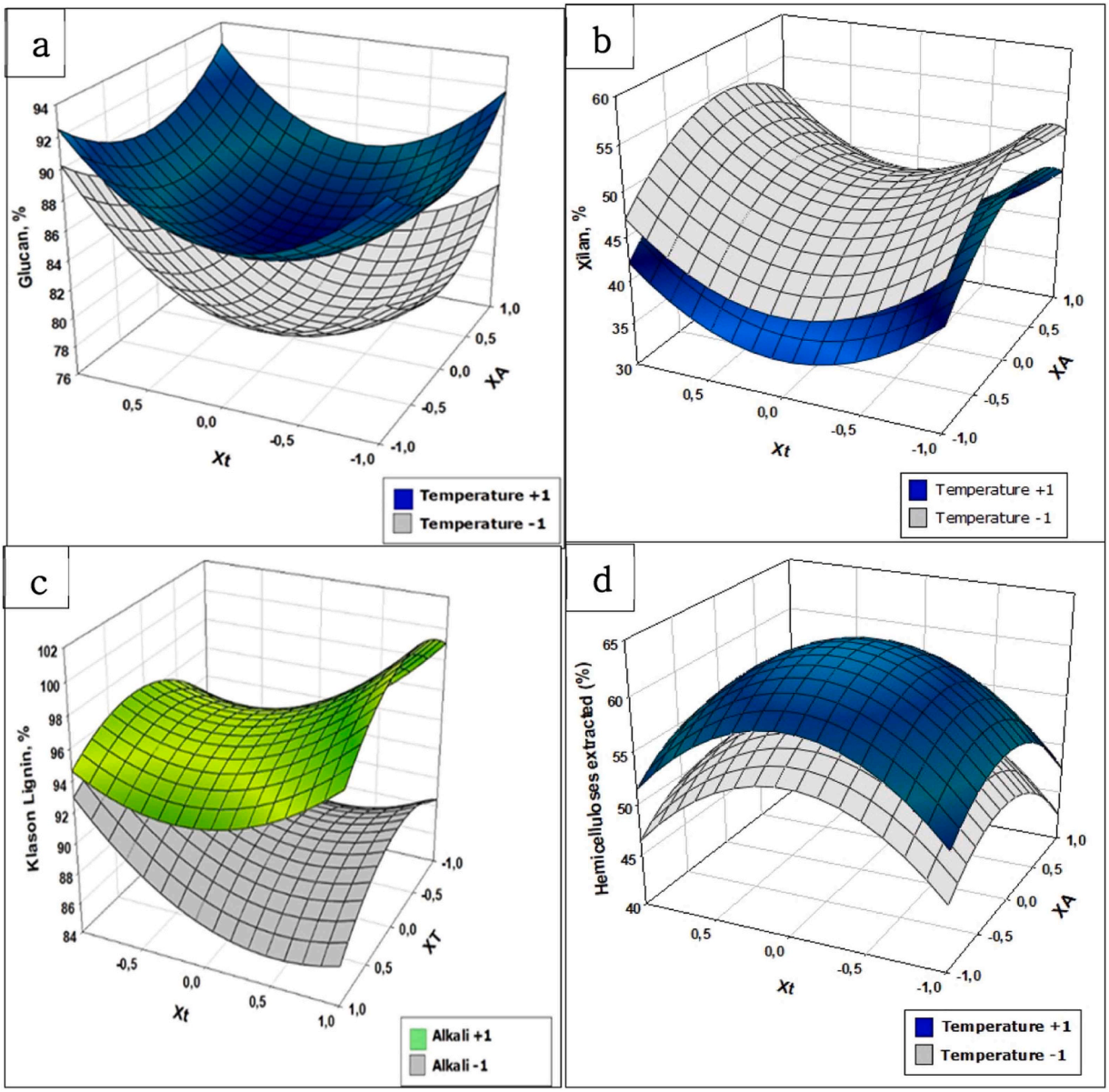

Fig. 1. Response surfaces for variations in: a) glucan content; b) xylan content in the solid as a function of operating time and alkali concentration, for the maximum and minimum temperatures of the CAE process. c) Klason lignin content in the solid as a function of temperature and operating time for the maximum and minimum alkali concentrations of the CAE process. d) extracted hemicellulose content in the liquor as a function of alkali concentration and operating time, for maximum and minimum temperatures in the CAE process.

under constant stirring agitation. During the reaction, significant foam formation and a temperature increase were observed. This phenomenon can be attributed to the energy released upon cleavage of the bonds linking cellulose with lignin and hemicelluloses (Katz, 1992). H_2O_2 acts as an oxidizing agent, breaking the chemical bonds within lignin and hemicellulose, facilitating their dissolution in the liquid phase. Sodium hydroxide (NaOH) from the prior CAE stage likely contributed by softening the cell wall, enhancing the accessibility of H_2O_2 to these target components.

Once foam generation dropped and the temperature stabilized (approximately 2 h), the solid and liquid phases were separated using vacuum filtration. The liquid fraction, enriched in hemicelluloses and lignins, was discarded. The remaining solid residue, anticipated to possess a cellulose content exceeding 80 %, was thoroughly washed with distilled water until the wash solution reached a neutral pH (6.5–7.5). The resulting material was oven-dried at 60°C for 24 h and subsequently characterized using FTIR (Fig. 4) and SEM (Fig. 3).

Following the AHP pretreatment, we employed a regioselective oxidation method using the TEMPO radical (2,2,6,6-tetramethylpiperidine-1-oxyl) to specifically target the primary hydroxyl group (C6) of the d-glucose repeating units (Ovalle-Serrano et al., 2018; Okita et al., 2010) The ultimate goal of this oxidation process is to assess the production of nanocellulose from the cellulosic ELM solid fraction. This oxidation induces the disaggregation and surface modification of cellulose microfibers, forming nanofibers due to the strong repulsive forces generated during the oxidation process. The initial reaction stage yields a homogeneous and translucent aqueous suspension of TEMPO-oxidized cellulose nanofibers (TOCN) in the form of sodium salt ($^{-}COO^{-}Na^{+}$). In this form, TOCN exhibits good dispersion in water due to the presence of ionic species: COO- groups on the cellulose surface and Na+ ions in the solution. These COO- -groups electrostatically repel each other (Coulombic repulsion), preventing hydrogen bond formation between nanofibers and promoting water dispersion. This phenomenon, so-called "hydrogen bond blocking," was clarified by Missoum (Missoum et al.,

2013). Their study discovered that adding NaCl to an aqueous suspension of TOCN interferes with the establishment of hydrogen bonds for redispersion of the material in water after lyophilization. The TEMPO oxidation process was successful in producing nanocellulose with excellent properties. Notably, the high purity of the obtained nanocellulose from Elm-CAE/AHP cellulose underscores the delignification step's effectiveness and the TEMPO radical's selectivity in targeting cellulose's aldehyde groups.

Figs. 2a and 2b compare the fibers of Elm-CAE/AHP with the final Elm nanocellulose obtained through TEMPO oxidation. The light cream color of the Elm-CAE/AHP fibers (Fig. 2a) is attributed to the AHP treatment, which removes residual lignin through the formation of a strong nucleophile (hydroperoxide ion, HOO^-). This ion converts the chromophoric functionalities in lignin to colorless derivatives. additionally, the reactive hydroxyl radical (·OH) and superoxide radical ($O_2^{\cdot -}$) produced during the AHP treatment help break down the substrate's interaction with lignin side chains, resulting in low molecular weight, water-soluble byproducts. (Su et al., 2015; Ho et al., 2019). This process effectively transforms the initially light brown Elm-CAE material into a whitish compound. Furthermore, we performed an ion exchange reaction using HCl to convert the $–COO^-Na^+$ groups in TOCN to their acid form (COOH). This process transformed the TOCN suspension into a homogeneous, semi-translucent, and non-flowing gel (Fig. 2). The observed change in physical properties is likely attributed to modifications in the hydrogen bonding network between TOCN-COO^-Na^+ and TOCN-COOH. Since COO^-Na^+ groups cannot participate in intra- and inter-nanofibrillar hydrogen bonding, their interactions in TOCN-COO^-Na^+ are restricted to hydroxyl group associations. In contrast, COOH groups can engage in both intra- and inter-nanofibrillar hydrogen bonding, reducing the hydrophilicity of TOCN-COOH compared to TOCN-COO^-Na^+.

Scanning electron microscopy (SEM) images in Fig. 3a-d show the morphological changes caused by CAE and AHP pretreatments on Elm fibers. Fig. 3a depicts the Elm-CAE fiber, while Fig. 3b shows the Elm-CAE/AHP fiber after AHP pretreatment and pulping treatment. These images highlight the changes in fiber structure after the removal of hemicellulose and lignin. This process reduces the fiber width to less than 100 μm and breaks down the hierarchical organization of macrofibrils, making it easier to separate individual microfibrils (Su et al., 2015). Delignification effectively lowers lignin content while increasing cellulose content from 42 % to over 80 %. The micrographs of the delignified material also reveal an "unraveling" of the fiber's macrostructure due to the chemical treatment. This initial breakdown of the fiber is crucial for increasing the yield of nanocellulose in subsequent steps. Figs. 3c and 3d show the characteristic network structures of freeze-dried elm nanocellulose (TOCNs) produced by TEMPO oxidation.

The images the fibrillar network structure characteristic of TOCNs, their nanometric size, and homogeneity, which are important factors for the improvement of their physicochemical properties. These networks are constituted by highly extended and entangled structures with diameters ranging between 30 and 100 nm and lengths stretching several micrometers. However, it is important to acknowledge that this may not represent the actual state of TOCNs in solution. SEM has two limitations that hinder the observation of the native structure of TOCNs. The application of metallic coatings during sample preparation can increase the apparent size of the nanomaterial and, solvent removal through lyophilization can induce self-aggregation processes in TOCNs. (Faradilla et al., 2016; Nechyporchuk et al., 2015; Chan et al., 2013). Despite these limitations, SEM images provide valuable evidence of the nanostructuring of fibers achieved through TEMPO radical action. Figs. 3c and 3d illustrate the characteristic network structures of freeze-dried elm nanocellulose (TOCNs) generated through TEMPO oxidation. The images reveal the fibrillar network structure classically associated with TOCNs, emphasizing their nanoscale sizes and homogeneity, which improve their physicochemical properties. The networks are comprised of long and highly entangled structures, as evidenced by diameters of 30–100 nm and lengths of more than several micrometers. That said, this may not represent the true state of TOCNs in solution. There are two fundamental limitations of scanning electron microscopy (SEM) that make it challenging to investigate the intrinsic structure of TOCNs. The application of metallic coatings during sample preparation can increase the apparent size of the nanomaterial, while solvent removal through lyophilization can induce self-aggregation processes in TOCNs (Faradilla et al., 2016; Nechyporchuk et al., 2015; Chan et al., 2013). Despite these limitations, SEM images provide valuable evidence of the nanostructuring of fibers achieved through TEMPO radical action.

Figs. 4a and 4b present the FTIR spectra of untreated Elm fiber (black line), Elm-CAE, Elm-CAE/AHP fibers (red and green lines, respectively), and Elm-CAE/AHP-TEMPO (blue line). The spectra reveal significant differences between untreated Elm, Elm-CAE, and Elm-CAE/AHP fibers, particularly in regions associated with hemicelluloses and lignin. The spectra can be analyzed in three regions: the first between 3400–2800 cm^{-1} , the second between 1800–1000 cm^{-1} , and the final fingerprint region below 900 cm^{-1} . The broad stretching vibration band observed at 3400–3000 cm^{-1} is attributed to O-H groups, while the medium and weak band around 2800–3000 cm^{-1} corresponds to asymmetric and symmetric stretching C-H vibrations in xylose, cellulose, and lignin structures. The bands between 1740–1510 cm^{-1} are associated to olefinic C═C and C═O vibrations in aromatic structures. Bending vibrations in the ranges of 1460–1325 and 900–750 cm^{-1} are assigned to

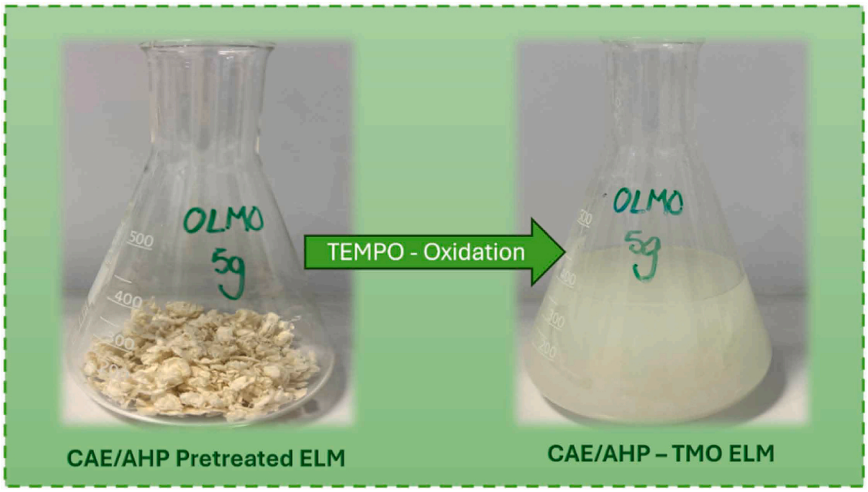

Fig. 2. Schematic illustration of TEMPO treatment on ELM-CAE/AHP fibers.

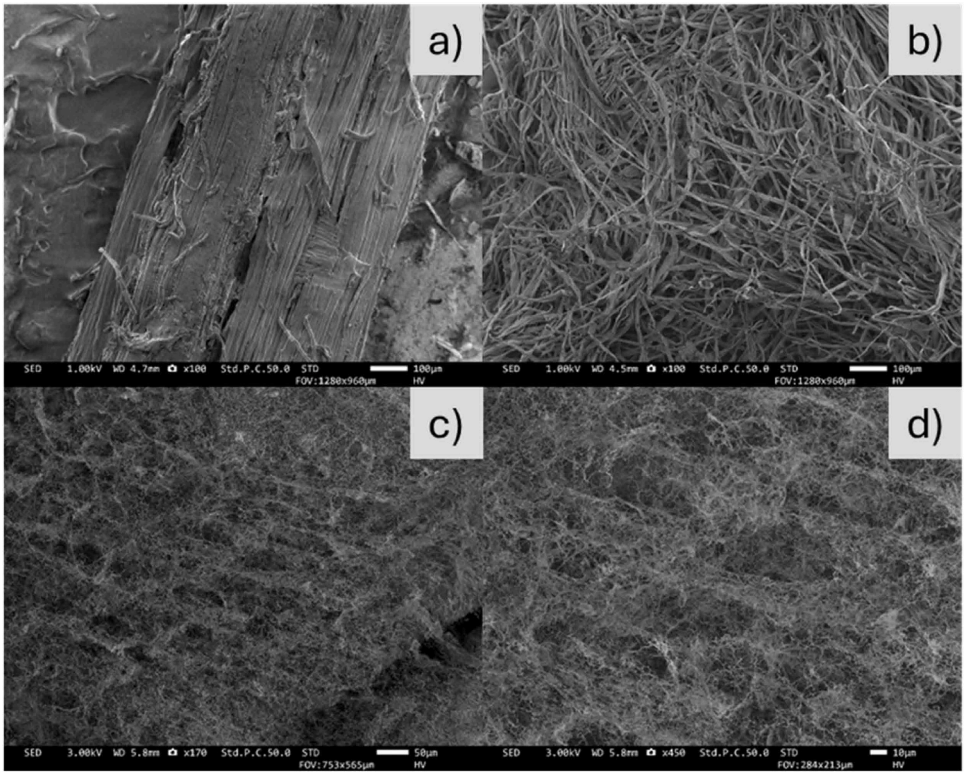

Fig. 3. SEM images of (a) ELM-CAE treated, (b) ELM-CAE/AHP treated, and (c, d) TOCNF from ELM-CAE/AHP fibers. Scale bars are 100 μm in figures (a) and (b), 50 μm in (c), and 10 μm in (d).

C-H, while the strong C-O stretching vibrations are observed between 1280–1030 cm^{-1} . As shown in Table 4, all samples exhibited similar spectra with many common functional groups.

Notably, the bands at 1731 cm^{-1} and 1240 cm^{-1} , corresponding to carbonyl (C═O) stretching vibrations in lignin and C-O-C vibrations in aromatic ether linkages of lignin, respectively, are significantly reduced or absent in the Elm-CAE/AHP fiber spectrum. This observation confirms the successful removal of lignin and hemicelluloses by the combined CEA and AHP treatment. Studies suggest that alkaline conditions generally promote higher lignin removal yields (Liu et al., 2021). On the other hand, the characteristic cellulose signals are present and common to all spectra. These include the broad band between 3650 and 3000 cm^{-1} (1) corresponding to O-H stretching vibrations, the C-H stretching vibration at 2901 cm^{-1} (3), the C6-H2 bending between 1424 and 1315 cm^{-1} , the C-O-C stretching vibration at 1160 cm^{-1} , the characteristic C-O vibration (from C2, C3, and C6) at 1055–1032 cm^{-1} , and the anomeric carbon C1-H vibration around 900 cm^{-1} (Sidi-Yacoub et al., 2019)

The TOCN-COOH spectrum (blue line) closely resembles that of cellulose. It indicates that no new bonds were formed during the oxidation process, except for a characteristic peak at 1722 cm^{-1} , attributed to the C═O stretching vibration in free carboxylic acids Fig. 4b. This peak confirms the successful surface oxidation of Elm-CAE/AHP fibers through TEMPO treatment. Importantly, this peak was absent in the Elm-CAE/AHP fiber spectrum due to the removal of lignin and hemicelluloses, which may have masked the signal. The presence of the peak in TOCN-COOH confirms the effectiveness of TEMPO oxidation in introducing carboxylic acid groups onto the surface of cellulose nanofibers, thereby modifying their structure and properties. The spectra for all three stages of Elm fiber treatment for nanocellulose production show the presence of other characteristic cellulose signals, suggesting that TEMPO oxidation primarily modifies the surface chemistry of nanofibers without affecting the fundamental structure of cellulose itself.

Furthermore, from the FTIR data, we estimated important structural parameters like the Total Crystallinity Index (TCI), Hydrogen Bonding Index (HBI) (Kruer-Zerhusen et al., 2018), and Lignin Index (LI). The results are presented in Table 5. The results indicate a steady rise in crystallinity (TCI) throughout the treatments, implying structural reorganization and improved molecular packing in the cellulose. The untreated ELM sample had the lowest TCI (0.910), whereas the Elm CAE/AHP/TEMPO-treated one had the highest TCI (0.977). This was observed to reveal that the application of chemical treatments, particularly the AHP and TEMPO oxidation treatment, improved the cellulose crystallinity and ordering.

In the case of HBI, a visible difference is observed. The application of CAE treatment caused the decrease of HBI to 0.880, a process that can be attributed to the partial disruption of hydrogen bonds due to delignification. However, as the samples underwent subsequent treatments (AHP and TEMPO), HBI values increased again, finally reaching 0.958 in the final stage, which can indicate a reformation or restructuring of hydrogen bonds after the removal and oxidation of lignin. The Lignin Index (LI) shows a significant reduction after chemical treatments. The untreated sample had the highest LI (1.570), confirming a high lignin content. With each successive treatment, the LI value progressively decreased, with the lowest LI (1.078) observed in the Elm CAE/AHP/TEMPO sample. This confirms the effectiveness of the applied treatments in removing lignin, with TEMPO oxidation playing a crucial role in the final stage. Data suggest that the applied treatments not only enhanced cellulose crystallinity but also effectively removed lignin, leading to structural modifications that could improve the material's performance in further applications, such as nanocellulose production. The stability of TOCN dispersions in water is directly linked to the extent of surface modification, measured by the number of carboxylic acid groups introduced during TEMPO oxidation. To quantify this modification (degree of oxidation, DO), we employed conductometric titration with a standard sodium hydroxide (NaOH) solution. This technique measures the carboxylate content of TOCN-COOH derived from Elm-

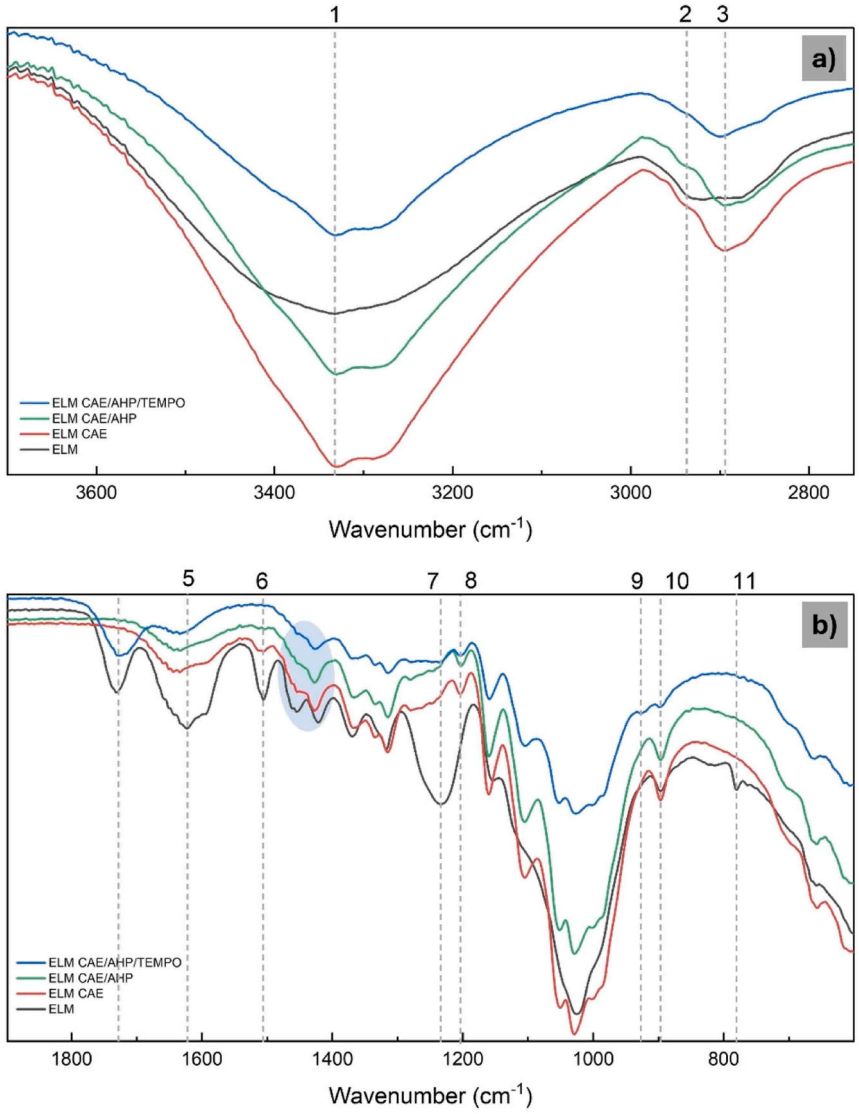

Fig. 4. Fourier Transform Infrared (FTIR) spectra of the Elm-CAE treated, Elm-CAE/AHP treated and, TOCNF from Elm-CAE/AHP fibers. a) region from 3800 to 2800 cm^{-1} and b) region from 1800 to 700 cm^{-1}.

Table 4
FTIR spectral peak assignments for Elm-CAE treated, Elm-CAE/AHP treated and, TOCNF from Elm-CAE/AHP fibers.

Band	Wavenumber (cm^{-1})	Lignin	Hemicellulose	Cellulose	Nanocellulose	Assignment
1	3700–3100	X	X	X	X	O–H stretching vibration of hydrogen-bonded hydroxyl groups
2	2930	X				C–H stretching in aromatic methoxyl groups, methyl, and methylene groups of side chains; also observed in alkanes and alkenes
3	2895	X	X	X	X	Symmetric and asymmetric C–H stretching vibrations in CH, CH_2, and CH_3 groups
4	1729		X		X	C═O stretching vibration of protonated COOH groups (nanocellulose) and acetyl fragments (hemicellulose)
5	1622–1690	X				Bending vibrations of crystallization water. This peak has three main contributions that change significantly after treatments; one is associated with lignin ring stretching near 1690 cm^{-1}
6	1505	X	X			Aromatic skeletal vibrations at 1505 cm^{-1} and 1426 cm^{-1} , along with C–H deformation and aromatic ring vibrations at 1462 cm^{-1} , characteristic of all lignins. Also includes scissor-symmetric C–H bending vibrations in CH_2 groups of hemicellulose
7	1280–1030	X	X	X	X	C–O stretching vibrations found in alcohols, phenols, esters, and ethers
8						C-O (υ) Alcohol, phenol, ester, ether"
9	926				X	β−1,4-glycosidic C–O–C stretching
10	895	X	X	X	X	Asymmetric β−1,6-glycosidic stretching
11	780	X				O–H out-of-plane bending

Table 5
Evolution of crystallinity parameters derived from FTIR data for Elm-CAE treated fibers, Elm-CAE/AHP treated fibers, and TOCNF obtained from Elm-CAE/AHP fibers.

SAMPLE	TCI	HBI	LI
ELM	0.910	0.990	1.570
ELM CAE	0.961	0.880	1.117
ELM CAE/AHP	0.972	0.906	1.102
ELM CAE/AHP/TEMPO	0.977	0.958	1.078

CAE/AHP fibers The carboxylate content and D.O were calculated using the equations proposed by Fras et al. (2005). Fig. 5c depicts a segment of the conductometric titration curve for the TEMPO oxidation of Elm-CAE/AHP fibers with additional ultrasound treatment. The plateau observed between 63.42 and 72.19 mL (Fig. 5c) corresponds to the neutralization of carboxyl groups by NaOH. This translates to a DO of 0.3 and a carboxylate content of 1.75 mmol/g for the obtained TOCN-COOH.

Interestingly, the carboxylate content (1.75 mmol/g) of TOCN-COOH from Elm-CAE/AHP fibers (delignified and ultrasound-treated during TEMPO) is comparable to or even higher than values reported for TOCN from other lignocellulosic sources. For instance, studies on hemp, commercial bamboo pulp, and bleached kraft pulp from bagasse yielded TOCN with carboxylate contents ranging from 1.5 to 1.7 mmol/g (Plengnok, Jarukumjorn, 2020; Gupta et al., 2019) Similarly, TOCN obtained from eucalyptus, ginkgo, and rice straw exhibited carboxylate contents between 0.8 and 1.4 mmol/g and 1.3–1.6 mmol/g depending on the applied NaClO concentration (low: 5 mmol; high: 10 mmol) during TEMPO oxidation (Boschetti et al., 2021; Jiang et al., 2013).

Zeta potential (ζ) serves as a valuable indicator for evaluating the stability of aqueous TOCN dispersions. This parameter reflects the magnitude of electrostatic repulsion between particles. Low absolute values of zeta potential (between 0 mV and ±30 mV) suggest a higher tendency for aggregation due to dominant attractive forces. Conversely, high absolute values (above ±40 mV) indicate stable dispersions over time. (Faradilla et al., 2016, 2017; Li et al., 2017). Fig. 5a shows the zeta potential values for TOCN-COOH dispersions derived from Elm-CAE/AHP fibers with ultrasound treatment during TEMPO oxidation. As expected, due to the high carboxylate content, the zeta potential exhibits a high negative value (-45 mV). These results support the notion that delignification and ultrasound application during TEMPO oxidation enhance the introduction of carboxylic groups on the cellulose surface. This, in turn, leads to stronger electrostatic repulsion and superior stability of TOCN-COOH dispersions obtained from Elm-CAE/AHP fibers. The zeta potential values for Elm-CAE/AHP fiber derived TOCN are comparable to or even surpass those reported for other TEMPO-oxidized TOCNs, such as corn stalk (-23 mV), bleached kraft pulp from softwood (-58 mV), and hydrolyzed cassava bagasse (-52 mV) (Hu et al., 2013).

Thermogravimetric analysis (TGA) in Fig. 6 revealed significant differences in thermal stability between the Elm-CAE/AHP and the Elm-CAE/AHP/TEMPO (TEMPO-oxidized cellulose nanofibers - TOCNF). The chemical pretreatment, evident from the presence of sodium carboxylate groups (confirmed by FTIR), reduced TOCNF's thermal stability. TOCNF degradation began nearly 100°C earlier (202°C) compared to Elm-CAE/AHP fibers (300°C). This is reflected in the DTG curves, where a single peak at 360°C indicates Elm-CAE/AHP fiber degradation, while TOCNF exhibits two distinct peaks at 260°C and 304°C. These findings align with prior research by Jiménez-López et al., (2020), on the thermal degradation mechanism of cellulose nanofibers. They proposed a three-stage mechanism for mechanically pretreated

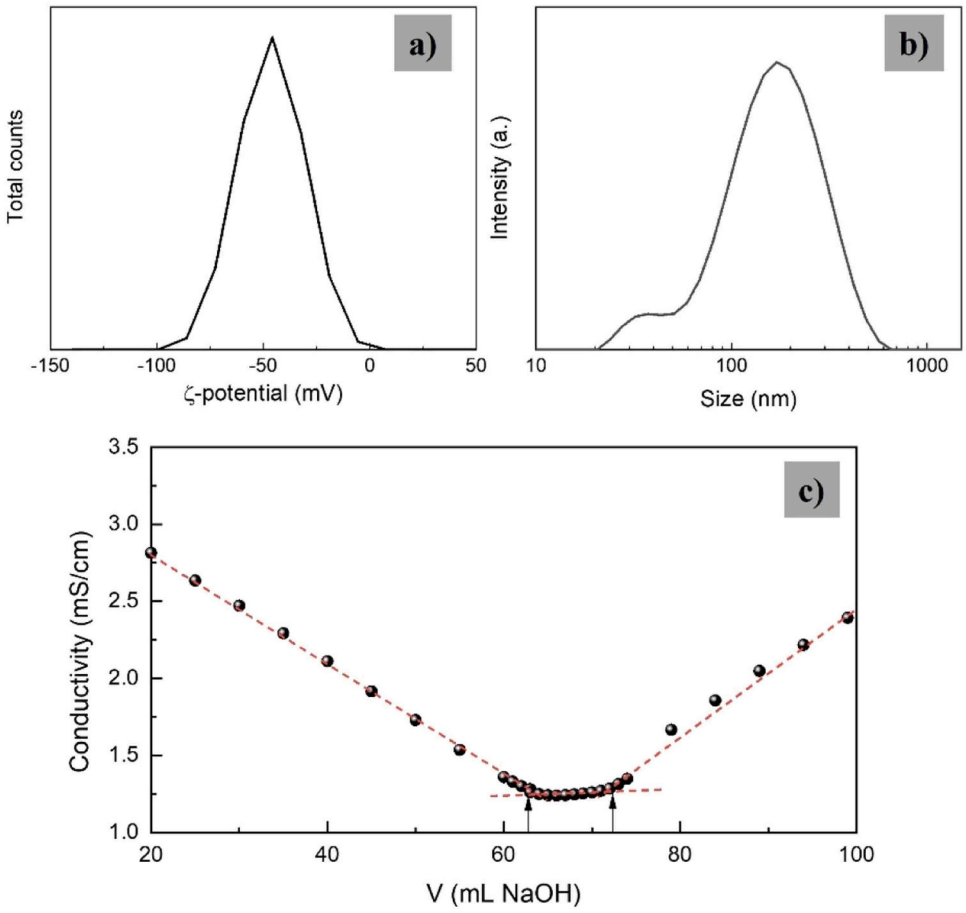

Fig. 5. z-potential (a), Size distribution (b), and conductimetric titration of TOCNF from Elm-CAE/AHP fibers.

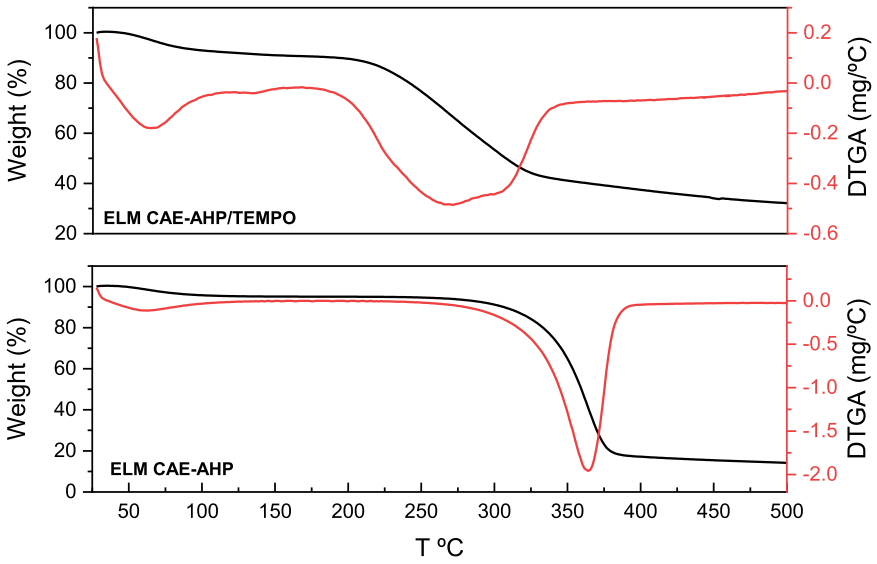

Fig. 6. Thermal stability of TOCNF from ELM-CAE/AHP fibers (thermogravimetric curves and first derivate curves).

CNF similar to cellulose pulp, involving water evaporation, cellulose structure breakdown, and char formation. However, the presence of sodium carboxylate groups in TOCNF introduces an additional degradation stage (150–250°C) involving decarboxylation and dehydration, followed by the established cellulose degradation stages.

The lower thermal stability limits the use of nanocellulose mostly to low-heat environments, but it remains effective in many low-temperature or ambient conditions such as waterborne barrier films, paper coatings, rheology modifiers, aerogels, and biomedical or cosmetic formulations. Applications involving prolonged or cyclic exposure to high temperatures—such as thermoplastic extrusion of biocomposites, high-power electronic substrates, or down-hole fluids in oilfield operations—would require additional steps (e.g., ion-cross-linking, esterification, silanisation, or incorporation into hybrid matrices) to protect the fibrils and preserve their mechanical and functional performance under those more demanding conditions.

4. Conclusions

In our comprehensive analysis employing cold alkaline extraction (CAE), alkaline hydrogen peroxide (AHP), TEMPO oxidation, FTIR analysis, SEM imaging, zeta potential measurement, conductometric titration, and thermogravimetric analysis (TGA) provides a holistic understanding of the structural and thermal characteristics of TOCNF.

The combination of CAE and AHP effectively removes residual lignin and hemicellulose, paving the way for subsequent TEMPO oxidation to modify the fiber surface. Measurements of FTIR, SEM, tehcniques like zeta potential and conductometric titration indicate enhanced dispersion stability and the effectiveness of surface modification. Finally, TGA highlights the influence of chemical pretreatment on thermal stability, with TOCNF exhibiting distinct degradation profiles compared to untreated fibers.

Collectively, these findings underscore the importance of a multifaceted approach for optimizing the properties of cellulose nanofibers. By tailoring the pretreatment process, researchers can achieve desired characteristics for diverse applications.

CRediT authorship contribution statement

J.M. Loaiza: Conceptualization, Methodology, Investigation, Writing – review & editing. **E.A. Gutiérrez:** Formal analysis, Software, Visualization, Writing – original draft. **J.C. García:** Funding acquisition, Project administration, Supervision, Validation. **F. López:** Methodology, Supervision, Writing – review & editing.

Declaration of Competing Interest

The authors declare that they have no known competing financial interests or personal relationships that could have appeared to influence the work reported in this paper.

Acknowledgements

The authors want to acknowledge the financial support from EPIT-Feder 2021–2027, University of Huelva, "Cascade biorefinery from agroforestry waste and energy crops within the framework of the circular economy" (EPIT1382023). And Spanish Ministry of Science, Innovation and Universities, Grant proyect: “Forest waste and high productivity hardwoods species hydrolytic and thermochemical biorefinery for obtaining value-added chemicals”, (REF: MICIIN PID2020-112875RB-C21), and Dr. Javier Mauricio Loaiza thanks a the co-funded by Junta of Andalusia (Spain) through post-doctoral Grant No. DC 21_00664.

Data availability

No data was used for the research described in the article.

References

Alaejos, J., Tapias, R., López, F., Romero, D., 2023. Biomass production and quality of twelve fast-growing tree taxa in short rotation under Mediterranean climate. Forests 14, 19994907. https://doi.org/10.3390/f14061156.

Alesso, S.P., Tapias, R., Alaejos, J., Fernández, M., 2021. Biomass yield and economic, energy and carbon balances of ulmus pumila L., robinia pseudoacacia L., and populus × euroamericana (Dode) guinier short-rotation coppices on degraded lands under Mediterranean climate. Forests 12, 19994907. https://doi.org/10.3390/f12101337.

Alfaro, A., López, F., Pérez, A., García, J.C., Rodríguez, A., 2010. Integral valorization of tagasaste (Chamaecytisus proliferus) under hydrothermal and pulp processing. Bioresour. Technol. 101, 7635–7640. https://doi.org/10.1016/j.biortech.2010.04.059.

Amorós, M.D.L.C., Mauri, P.V., Curt, M.D., 2021. Modificación de la actividad antioxidante de extractos de plantas mediante procesos enzimáticos. An. da Acad. Bras. De. Ciências 179, 1–14.

Bessaad, A., Bilger, I., Korboulewsky, N., 2021. Assessing biomass removal and woody debris in whole-tree harvesting system: are the recommended levels of residues ensured. Forests 12, 807. https://doi.org/10.3390/f12060807.

Boschetti, W.T.N., Carvalho, A.M.M.L., Carneiro, A. de C.O., Vidaurre, G.B., Gomes, F.J. B., Soratto, D.N., 2021. Effect of mechanical treatment of eucalyptus pulp on the

production of nanocrystalline and microcrystalline cellulose. Sustainability 13 (11), 5888. https://doi.org/10.3390/su13115888.
Caparrós, S., Ariza, J., López, F., Nacimiento, J.A., Garrote, G., Jiménez, L., 2008. Hydrothermal treatment and ethanol pulping of sunflower stalks. Bioresour. Technol. 99 (5), 1368–1372. https://doi.org/10.1016/j.biortech.2007.01.045.
Carvalho, D.M. de, Queiroz, J.H. de, Colodette, J.L., 2016. Assessment of alkaline pretreatment for the production of bioethanol from eucalyptus, sugarcane bagasse and sugarcane straw. Ind. Crops Prod. 94, 932–941. https://doi.org/10.1016/j.indcrop.2016.09.069.
Chan, C.H., Chia, C.H., Zakaria, S., Ahmad, I., Dufresne, A., 2013. Production and characterisation of cellulose and nano-crystalline cellulose from kenaf core wood. BioResources 8 (1), 785–794. https://doi.org/10.15376/biores.8.1.785-794.
Council of the European Union, 2023. Renewable energy: Council adopts new rules. Retrieved from. ⟨https://www.consilium.europa.eu/en/press/press-releases/2023/10/09/renewable-energy-council-adopts-new-rules/⟩.
Domínguez, E., Nóvoa, T., del Río, P.G., Garrote, G., Romaní, A., 2020. Sequential two-stage autohydrolysis biorefinery for the production of bioethanol from fast-growing paulownia biomass. Energy Convers. Manag 226, 113517.
EUFORGEN, 2025. Ulmus minor (European elm). European Forest Genetic Resources Programme (EUFORGEN). Available at: ⟨https://www.euforgen.org/species/ulmus-minor⟩. [Accessed 19 Mar. 2025].
European Parliament, 2020. Committee on agriculture and rural development. The challenge of land abandonment after 2020 and options for mitigating measures. European Parliament, Brussels. ⟨https://www.europarl.europa.eu/portal/en⟩.
Faradilla, R.H.F., Lee, G., Arns, J.Y., Roberts, J., Martens, P., Stenzel, M.H., Arcot, J., 2017. Characteristics of a free-standing film from banana pseudostem nanocellulose generated from TEMPO-mediated oxidation. Carbohydr. Polym. 174, 1156–1163. https://doi.org/10.1016/j.carbpol.2017.07.025.
Faradilla, R.H.F., Lee, G., Rawal, A., Hutomo, T., Stenzel, M.H., Arcot, J., 2016. Nanocellulose characteristics from the inner and outer layer of banana pseudo-stem prepared by TEMPO-mediated oxidation. Cellulose 23 (5), 3023–3037. https://doi.org/10.1007/s10570-016-1025-8.
Faradilla, R.F., Lucia, L., Hakovirta, M., 2020. Remarkable Physical and Thermal Properties of Hydrothermal Carbonized Nanoscale Cellulose Observed from Citric Acid Catalysis and Acetone Rinsing. Nanomaterials 10, 1049. https://doi.org/10.3390/nano10061049.
Feria, M.J., García, J.C., Pérez, A., Gomide, J.L., Colodette, J.L., López, F., 2012. Process optimization in kraft pulping, bleaching, and beating of leucaena diversifolia. Bioresources 7, 283–297.
Fernández, M., Alaejos, J., Andivia, E., Vázquez-Piqué, J., Ruiz, F., López, F., Tapias, R., 2018. Eucalyptus x urograndis biomass production for energy purposes: a logistical and economical approach to coordinating a biomass supply chain including energy characteristics. Biomass.. Bioenergy 111, 22–30. https://doi.org/10.1016/j.biombioe.2018.01.020.
Fernández, M., Alaejos, J., Andivia, E., Madejón, P., Díaz, M.J., Tapias, R., 2020. Short rotation coppice of leguminous tree leucaena spp. Improves soil fertility while producing high biomass yields in Mediterranean environment. Ind. Crops Prod. ⟨https://10.1016/j.indcrop.2020.112911⟩.
Fernández, M., Tapias, R., Camacho, V., Alaejos, J., 2023. Quality of the pellets obtained with wood and cutting residues of stone pine (Pinus pinea L.). Forests 14, 19994907. https://doi.org/10.3390/f14051011.
Ferreira, J.A., Brancoli, P., Agnihotri, S., Bolton, K., Taherzadeh, M.J., 2018. A review of integration strategies of lignocelluloses and other wastes in 1st generation bioethanol processes. Process Biochem. https://doi.org/10.1016/j.procbio.2018.09.006.
Fras, L., Johansson, L.S., Stenius, P., Laine, J., Stana-Kleinschek, K., Ribitsch, V., 2005. Analysis of the oxidation of cellulose fibres by titration and XPS. Colloids Surf. A Physicochem. Eng. Asp. 260 (1–3), 101–108. https://doi.org/10.1016/j.colsurfa.2005.01.035.
García, I.P., 2016. Evaluación de ulmus pumila L. Y populus spp. Como cultivos energéticos en corta rotación. Tesis Doctoral. Universidad Politécnica de Madrid, España.
García, J.C., Díaz, M.J., Garcia, M.T., Feria, M.J., Gómez, D.M., López, F., 2013. Search for optimum conditions of wheat straw hemicelluloses cold alkaline extraction process. Biochem. Eng. J. 71, 127–133. https://doi.org/10.1016/j.bej.2012.12.008.
Gupta, H., Kumar, H., Kumar, M., Gehlaut, A.K., Gaur, A., Sachan, S., Park, J.-W., 2019. Synthesis of biodegradable films obtained from rice husk and sugarcane bagasse to be used as food packaging material. Environ. Eng. Res. 25 (4), 506–514. https://doi.org/10.4491/eer.2019.191.
Haldar, D., Purkait, M.K., 2020. Lignocellulosic conversion into value-added products: a review. Process Biochem 89, 110–133. https://doi.org/10.1016/j.procbio.2019.10.001.
Ho, M.C., Ong, V.Z., Wu, T.Y., 2019. Potential use of alkaline hydrogen peroxide in lignocellulosic biomass pretreatment and valorization – a review. Renew. Sust. Energ. Rev. 112, 75–86. https://doi.org/10.1016/j.rser.2019.04.082.
Hu, L., Zheng, G., Yao, J., Liu, N., Weil, B., Eskilsson, M., Karabulut, E., Ruan, Z., Fan, S., Bloking, J.T., McGehee, M.D., Wågberg, L., Cui, Y., 2013. Transparent and conductive paper from nanocellulose fibers. Energy Environ. Sci. 6 (2), 513–518. https://doi.org/10.1039/c2ee23635d.
International Energy Agency (IEA), 2017. World Energy Outlook 2017. IEA. ⟨https://www.iea.org/reports/world-energy-outlook-2017⟩.
Jiang, F., Han, S., Hsieh, Y.L., 2013. Controlled defibrillation of rice straw cellulose and self-assembly of cellulose nanofibrils into highly crystalline fibrous materials. RSC Adv. 3 (30), 12366–12375. https://doi.org/10.1039/c3ra41646a.
Jiménez-López, L., Eugenio, M.E., Ibarra, D., Darder, M., Martín, J.A., Martín-Sampedro, R., 2020. Cellulose nanofibers from a Dutch elm disease-resistant ulmus minor clone. Polymers 12 (11), 1–21. https://doi.org/10.3390/polym12112450.
Katz, J., 1992. Alkaline hydrogen peroxide bleaching method. J. Pulp Pap. Sci.
Kruer-Zerhusen, N., Cantero-Tubilla, B., Wilson, D.B., 2018. Characterization of cellulose crystallinity after enzymatic treatment using Fourier transform infrared spectroscopy. Cellulose 25 (1), 37–48. https://doi.org/10.1007/s10570-017-1542-0.
Li, Z., Sathitsuksanoh, N., Zhang, W., Goodell, B., Renneckar, S., Biomaterials, S., Tech, V., Hall, C., Virginia, B., States, U., Engineering, C., Hall, E., 2017. Towards an understanding of cellulose microfibril dimensions from TEMPO-Oxidized pulp fiber. Nanocelluloses Prep. Prop. Appl. ACS Symp. Ser. https://doi.org/10.1021/bk-2017-1251.
Liu, X., Renard, C.M.G.C., Bureau, S., Le Bourvellec, C., 2021. Revisiting the contribution of ATR-FTIR spectroscopy to characterize plant cell wall polysaccharides. Carbohydr. Polym. 262, 117935. https://doi.org/10.1016/j.carbpol.2021.117935.
Loaiza, J.M., Alfaro, A., López, F., et al., 2019. Optimization of Laccase/Mediator system (LMS) stage applied in fractionation of eucalyptus globulus. Polymers 11, 731. https://doi.org/10.3390/polym11040731.
Loaiza, J.M., Alfaro, A., López, F., et al., 2020. Integral use of eucalyptus globulus in a double stage biorefinery scheme. Maderas Cienc. Tecnol. https://doi.org/10.4067/s0718-221x2020005000109.
Loaiza, J.M., López, F., García, M.T., Fernández, O., Díaz, M.J., García, J.C., 2016. Selecting the pre-hydrolysis conditions for eucalyptus wood in a fractional exploitation biorefining scheme. J. Wood Chem. Technol. 36, 211–223. https://doi.org/10.1080/02773813.2015.1112402.
Lokanathan, A., Madhavan, A., Rajesh, A., Vaidyanathan, R., Srinivasan, M., 2014. Cellulose nanocrystal-mediated synthesis of silver nanoparticles: role of sulfate groups in nucleation phenomena. Biomacromolecules 15 (1), 373–379. https://doi.org/10.1021/bm401613h.
López, F., Pérez, A., Zamudio, M.A.M., De Alva, H.E., García, J.C., 2012. Paulownia as raw material for solid biofuel and cellulose pulp. Biomass Bioenergy 45, 77–86. https://doi.org/10.1016/j.biombioe.2012.05.010.
Lozano-Calvo, S., Loaiza, J.M., Garcia, J.C., Garcia, M.T., Lopez, F., 2024. Ultrasound-assisted cold alkaline extraction: increasing hemicellulose extraction and energy production from populus wood. Forests 15 (109). https://doi.org/10.3390/f15010109.
Mishra, S.P., Thirree, J., Manent, A.S., Chabot, B., Daneault, C., 2011. Ultrasound-catalyzed TEMPO-mediated oxidation of native cellulose for the production of nanocellulose: effect of process variables. BioResources 6 (1), 121–143. https://doi.org/10.15376/biores.6.1.121-143.
Missoum, K., Belgacem, M.N., Bras, J., 2013. Nanofibrillated cellulose surface modification: a review. Materials 6, 1745–1766. https://doi.org/10.3390/ma6051745.
MTERD (Ministerio para la Transición Ecológica y el Reto Demográfico)., 2022. Mitigación, políticas y medidas en el sector agrícola. Gobierno de España. ⟨https://www.miteco.gob.es/es/cambio-climatico/temas/mitigacion-politicas-y-medidas/agricola.aspx⟩.
Nechyporchuk, O., 2015. Cellulose nanofibers for the production of bionanocomposites. https://theses.hal.science/tel-01244186v1.
Nicolescu, V.N., Rédei, K., Mason, W.L., Vor, T., Pöetzelsberger, E., Bastien, J.-C., Brus, R., Benčať, T., 2020. Ecology, growth and management of black locust (Robinia pseudoacacia L.), a non-native species integrated into european forests. J. For. Res. 31, 1081–1101. https://doi.org/10.1007/s11676-020-01116-8.
Okita, Y., Saito, T., Isogai, A., 2010. Entire surface oxidation of various cellulose microfibrils by TEMPO mediated oxidation. mL 100, 1696–1700.
Oliveira, N., del Río, M., Forrester, D.I., Rodríguez-Soalleiro, R., Bravo-Oviedo, A., 2018. Efectos de la gestión forestal en la biodiversidad y la estructura del bosque en plantaciones de eucalyptus globulus en el noroeste de España. For. Ecol. Manag. 410, 48–55.
Ovalle-Serrano, S.A., Gómez, F.N., Blanco-Tirado, C., Combariza, M.Y., 2018. Isolation and characterization of cellulose nanofibrils from Colombian fique decortication by-products. Carbohydr. Polym. 189, 169–177. https://doi.org/10.1016/j.carbpol.2018.02.031.
Pan, X., Sano, Y., 2005. Fractionation of wheat straw by atmospheric acetic acid process. Bioresour. Technol 96 (11), 1256–1263. https://doi.org/10.1016/j.biortech.2004.10.018.
Pérez, I., Pérez, J., Carrasco, J., Ciria, P., 2014. Respuestas del olmo siberiano a diferentes condiciones de cultivo bajo un sistema de corta rotación en áreas mediterráneas. Turk. J. Agric. For. 38, 652–662.
Plengnok, U., Jarukumjorn, K., 2020. Preparation and characterization of nanocellulose from sugarcane bagasse. Biointerface Res. Appl. Chem. 10 (3), 5675–5678. https://doi.org/10.33263/BRIAC103.675678.
Reiner, R.S., Rudie, A.W., 2017. Experiences with scaling-up production of TEMPO-Grade cellulose nanofibrils. Nanocelluloses Prep. Prop. Appl. 227–245. https://doi.org/10.1021/bk-2017-1251.ch012.
Reshmy, R., Philip, E., Madhavan, A., Arun, K.B., Binod, P., Pugazhendhi, A., Awasthi, M. K., Gnansounou, E., Pandey, A., Sindhu, R., 2021. Promising eco-friendly biomaterials for future biomedicine: cleaner production and applications of nanocellulose. Environ. Technol. Innov. 24, 1–33. https://doi.org/10.1016/j.eti.2021.101855.
Salas, C., Nypelö, T., Rodriguez-Abreu, C., Carrillo, C., Rojas, O.J., 2014. Nanocellulose properties and applications in colloids and interfaces. Curr. Opin. Colloid Interface Sci. 19 (5), 383–396. https://doi.org/10.1016/j.cocis.2014.10.003.
Sánchez, R., Rodríguez, A., García, J.C., Rosal, A., Jiménez, L., 2011. Exploitation of hemicellulose, cellulose and lignin from hesperaloe funifera. In: Bioresour. Technol, 102, pp. 1308–1315. https://doi.org/10.1016/j.biortech.2010.08.084.

Schild, G., Patt, R., Janzon, R., Kruse, T., Kordsachia, O., 2010. Multifunctional alkaline pulping, delignification and hemicellulose extraction. In: Cellulose Chem. Technol, 44, pp. 35–45.

Sidi-Yacoub, B., Oudghiri, F., Belkadi, M., Rodríguez-Barroso, R., 2019. Characterization of lignocellulosic components in exhausted sugar beet pulp waste by TG/FTIR analysis. In: J. Therm. Anal. Calorim, 138, pp. 1801–1809. https://doi.org/10.1007/s10973-019-08179-8.

Sixto, H., Cañellas, I., van Arendonk, J., Ciria, P., Camps, F., Sánchez, M., González, R., García, D., Martín, M., 2015. Growth potential of different species and genotypes for biomass production in short rotation in Mediterranean environments. For. Ecol. Manag. 354, 291–299.

Srirangan, K., Akawi, L., Moo-Young, M., Chou, C.P., 2012. Appl. Energy 100, 172–186.

Su, Y., Du, R., Guo, H., Cao, M., Wu, Q., Su, R., Qi, W., He, Z., 2015. Fractional pretreatment of lignocellulose by alkaline hydrogen peroxide: characterization of its major components. Food Bioprod. Process. 94 (March 2013), 322–330. https://doi.org/10.1016/j.fbp.2014.04.001.

TAPPI 211 om-02, 2002. Ash in wood, pulp, paper and paperboard: combustion at 525 °C. TAPPI Press, Atlanta, GA, USA.

TAPPI T222 om-11, 2011. Acid-insoluble lignin in wood and pulp. TAPPI Press, Atlanta, GA, USA.

TAPPI T249 cm-09, 2009. Carbohydrate composition of extractive-free wood and wood pulp by gas-liquid chromatography. TAPPI Press, Atlanta, GA, USA.

TAPPI T264 cm-07, 2007. Preparation of wood for chemical analysis. TAPPI Press, Atlanta, GA, USA.

Torres, F., González, R., Rodríguez, L., López, M., Pérez, L., 2019. Bacterial cellulose nanocomposites: an all-nano type of material. Mater. Sci. Eng. C. 98, 1277–1293. https://doi.org/10.1016/j.msec.2019.01.064.

Vanbeveren, S., Schweier, J., Berhongaray, G., Ceulemans, R., 2015. Operational short rotation woody crop plantations: manual or mechanised harvesting. Biomass.. Bioenergy 72, 8–18. https://doi.org/10.1016/j.biombioe.2014.11.019.

Velvizhi, G., Balakumar, K., Shetti, N.P., Ahmad, E., Kishore Pant, K., Aminabhavi, T.M., 2022. Integrated biorefinery processes for conversion of lignocellulosic biomass to value added materials: paving a path towards circular economy. Bioresour. Technol. 343 (September 2021), 126151. https://doi.org/10.1016/j.biortech.2021.126151.

Yetiş, F., Göktürk, B., Hocaoglu, F., Bakkar, R., Sargin, I., Akkaya, E., Akin, B., Yıldız, U., 2020. Acetylation of lignin containing microfibrillated cellulose and its reinforcing effect for polylactic acid. Eur. Polym. J. 134, 109803. https://doi.org/10.1016/j.eurpolymj.2020.109803.